Enhancing Inductive Operation of Low-Capacitance Cascaded H-Bridge StatComs Using Optimal Third-Harmonic Circulating Current

Ezequiel Rodriguez, *Student Member, IEEE*, Ramon Leyva, *Senior Member, IEEE*, Liu Qingxiang, *Student Member, IEEE*, Christopher D. Townsend, *Member, IEEE*, Glen G. Farivar, *Senior Member, IEEE*, Salvador Ceballos, and Josep Pou, *Fellow, IEEE*

***Abstract*—The cascaded H-bridge (CHB) low-capacitance static compensator (LC-StatCom) has a limited operating range in the inductive region compared to a conventional StatCom due to the inherent large oscillations on the capacitor voltages. This limitation constitutes a great drawback of CHB LC-StatComs. This article presents an effective hardware-free solution to overcome this drawback. The proposed solution is based on the injection of an optimal third-harmonic circulating current to suitably shape the capacitor voltages aiming at avoiding overmodulation. Considering all the effects of the third-harmonic circulating current, the article proposes a reference design that guarantees a prescribed safe operating voltage limit, thus increasing the operational range of the LC-StatCom. The proposed approach takes into account the inherent induced oscillation on the capacitor voltages. This approach has been verified by simulation and experimentally with a laboratory prototype, corroborating the excellent performance that agrees with the theoretical analysis.**

***Index Terms*—Arm current, capacitor voltage ripple, cascaded H-bridge (CHB), circulating current control, multilevel converter, static compensator (StatCom), zero-sequence current injection.**

Manuscript received August 3, 2020; revised October 28, 2020 and January 5, 2021; accepted February 25, 2021. Date of publication March 3, 2021; date of current version June 1, 2021. This work was supported by the Singapore Ministry of Education Academic Research Fund Tier 1 under Grant 2017-T1-001-213 (RG 90/17), and in part by the NTU Start-Up Grant #000603-00001: Compact and Reliable Power Converters. Recommended for publication by Associate Editor K. Wada. *(Corresponding author: Ezequiel Rodriguez.)*

Ezequiel Rodriguez and Josep Pou are with the School of Electrical and Electronic Engineering, Nanyang Technological University, Singapore 639798, Singapore (e-mail: ezequiel001@e.ntu.edu.sg; josep.pou@ieee.org).

Ramon Leyva is with the Departament d'Enginyeria Electrònica, Elèctrica i Automàtica,Universitat Rovira i Virgili, 43007 Tarragona, Spain (e-mail: ramon.leyva@urv.cat).

Liu Qingxiang is with the Energy Research Institute @ NTU, Interdisciplinary Graduate School, Nanyang Technological University, Singapore 639798, Singapore (e-mail: qingxian001@e.ntu.edu.sg).

Glen G. Farivar is with the Energy Research Institute @ NTU, Nanyang Technological University, Singapore 639798, Singapore (e-mail: gh_farivar@hotmail.com).

Christopher D. Townsend is with the Department of Electrical, Electronic and Computer Engineering, University of Western Australia, Crawley, WA 6009, Australia (e-mail: townsend@ieee.org).

Salvador Ceballos is with the Tecnalia, Basque Research and Technology Alliance, 48160 Derio, Spain (e-mail: salvador.ceballos@tecnalia.com).

Color versions of one or more of the figures in this article are available online at https://doi.org/10.1109/TPEL.2021.3063908.

Digital Object Identifier 10.1109/TPEL.2021.3063608

I. Introduction

LOW-CAPACITANCE static compensators (LC-StatComs) based on the cascaded H-bridge (CHB) multilevel converter have been recently proposed [1]–[6], showing reductions of approximately 80% in required energy storage capacity with respect to conventional CHB StatComs. The fact of being able to use reduced capacitance values allows reducing the converter size and cost for a given rated power or replacing the traditionally used electrolytic capacitors by more reliable technologies, such as film-type capacitors [7]–[9], which generally exhibit very low equivalent series resistance values. Smaller capacitances implicate time-varying capacitor voltages with relatively large oscillations [10], [11]. These oscillations have been proven to provide benefits in terms of efficiency and ac-side waveform quality when working in the capacitive region [12]–[14]. Nonetheless, the induced oscillation on the capacitor voltages yields overmodulation issues when working at certain power ranges in the inductive mode [2], [15], [16], because the ac-side converter voltage references overlap the capacitor voltage waveforms. The reduced operational range in the inductive mode is considered the main drawback of the LC-StatComs compared with conventional StatComs.

In order to overcome the aforementioned shortcoming, Farivar *et al.* [15], [16] report a passive reactive compensated single-phase LC-StatCom system. The concept consists of adding a series thyristor-bypassed-reactor to increase the voltage drop between the grid and the LC-StatCom when injecting inductive power. The larger voltage drop, reported in approaches [15], [16], increases the operating range in the inductive mode at the expense of adding extra hardware.

A different solution to the limited operating area in the inductive region is presented in [17], where a dc-link voltage shaping method for single-phase CHB LC-StatComs with energy storage integration is used. By suitably controlling the output current of a dc–dc converter, the dc-link capacitor voltage waveform can be shaped as desired regardless of the operating point. Therefore, the operating range in the inductive mode is increased at the expense of adding a power processing subunit by the dc–dc stage. The solution is especially suited for enhanced StatCom applications, in which the StatCom is integrated with either a

renewable energy source or an energy storage system, as the additional hardware needed is already installed.

The previous approaches were aiming at finding a solution to apply on each individual phase. Utilizing the flexibilities of a three-phase system with the purpose of increasing the operation range to full inductive mode was explored in [6]. A third-harmonic zero-sequence voltage was added to the three ac-side converter voltages of an LC-StatCom with star configuration. Specifically, Niu *et al.* [6] present a method to derive the optimal value of the third-harmonic voltage that minimizes the average value of the voltages in the capacitors, which, in turn, reduces the switching losses, as in [5]. Unlike [6], the proposed method minimizes the magnitude of the third-harmonic zero-sequence current in a delta-connected system in order to minimize the conduction losses.

This article proposes a novel compensation method based on circulating current injection for three-phase LC-StatComs with delta configuration [18]–[22] with the purpose of increasing the operation range to full inductive mode. Despite the fact that the proposed method is described for delta configuration, this approach can be readily extended to an LC-StatCom with star configuration. However, adapting the proposed method to the CHB-StatCom with star configuration should consider using the dual variable of the circulating current, i.e., the zero-sequence voltage [23].

Unlike the aforementioned solutions in [15]–[17], no extra hardware is needed. The aim of the circulating current is to adequately shape the capacitor voltages in such a way that overmodulation is avoided without increasing the voltage rating throughout the entire range of operation. To do so, a constrained optimization problem that minimizes the circulating current magnitude is proposed and solved analytically. Moreover, the article describes the calculation of the main reference waveforms taking into account the third-harmonic circulating current injection. Specifically, the shaped capacitor voltage references, ac-side converter voltage references, and shaped modulating signal references are calculated according to the third-harmonic injection.

The rest of this article is organized as follows. In Section II, the modeling of the LC-StatCom with delta configuration is reviewed, where the main steady-state relationships are presented. The section also describes the operational limit of LC-StatComs in the inductive mode. Based on the model, an optimal third-harmonic circulating current injection method to expand the inductive operation range is described in detail in Section III. Specifically, the shaped state trajectory, constraint modeling, and the resultant constrained optimization problem are addressed in detail. Section IV quantifies the power loss and current stress incurred. Section V provides experimental results that corroborate the excellent performance of the proposed approach. In addition, complementary simulation results, which show multilevel waveforms, are presented in Section VI. Finally, Section VII concludes this article.

II. Model of LC-StatCom With Delta Configuration

This section reviews the topology of LC-StatCom with delta configuration, its state variables, and its main mathematical relationships. Also, the main operational limit of the LC-StatCom in the inductive mode, when no circulating current is injected, is reviewed.

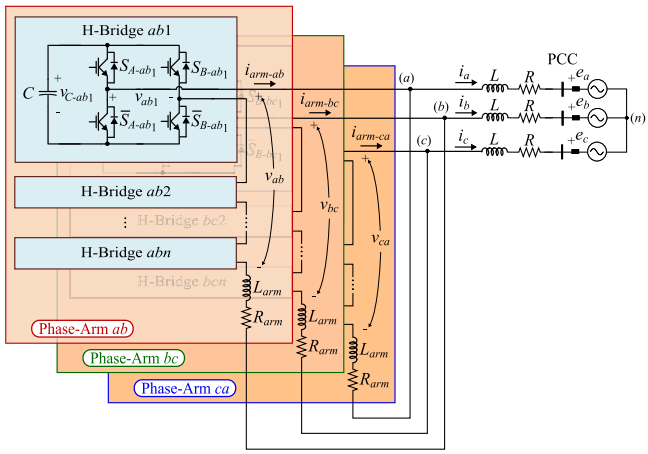

Fig. 1. Circuit diagram of a three-phase CHB power converter with delta configuration.

A. Topology

Fig. 1 shows a circuit representation of an LC-StatCom with delta configuration. The power converter consists of three identical phase arms $x \in \mathcal{X} = \{ab,\ bc,\ ca\}$. Each phase arm includes n series-connected H-bridges $j \in \mathcal{J} = \{1,\ 2, \ldots,\ n\}$ and an arm inductor L_{arm}. Each H-bridge consists of a floating capacitor C at its dc side and two pairs of power switches that work in a complementary manner, which provides three different output voltage levels. The three ac terminals of the power converter (a), (b), and (c) are connected to the point of common coupling (PCC), where the grid voltages are indicated as $e_a,\ e_b,\ e_c$. In the model, also an inductor L to filter the line currents is considered. Losses are modeled as series resistances R and R_{arm} in the line and in the arm, respectively, as depicted in Fig. 1.

B. Steady-State Relationships in CHB Multilevel Converters With Delta Configuration

In this subsection, for the sake of completeness, the main mathematical relationships of a CHB multilevel converter with delta configuration are revisited.

The cluster voltage reference $v^{\star}_{\Sigma-x}$ is defined as the sum of capacitor voltage references in a phase arm, i.e.,

$$v^{\star}_{\Sigma-x} = \sum_{j\in\mathcal{J}} v^{\star}_{C-xj} \tag{1}$$

where $v^{\star}_{C-xj}$ is the capacitor voltage reference in the jth H-bridge for the xth phase arm.

In addition, each phase-arm converter voltage reference $v^{\star}_{x}$ in the averaged model is related to its corresponding cluster voltage reference $v^{\star}_{\Sigma-x}$ as

$$v^{\star}_{x} = \delta^{\star}_{x} v^{\star}_{\Sigma-x} \tag{2}$$

where $\delta^{\star}_{x} \in [-1,\ 1]$ stands for the modulating signal reference [24]. This assumes that the capacitor voltage references are

balanced within the converter phase arm, i.e., $v^{\star}_{C-xj} = v^{\star}_{\Sigma-x}/n$, $\forall j,\ x$ [25]–[28].

The grid current references $i^{\star}_a$, $i^{\star}_b$, and $i^{\star}_c$ are linear combinations of the arm current references $i^{\star}_{\text{arm}-ab}$, $i^{\star}_{\text{arm}-bc}$, and $i^{\star}_{\text{arm}-ca}$. However, the transformation matrix of line currents to arm currents is nonfull rank. When introducing the circulating current reference $i^{\star}_{\text{circ}}$ as a constraint of arm current references [18], [21]

$$i^{\star}_{\text{circ}} = \frac{1}{3}\left(i^{\star}_{\text{arm}-ab} + i^{\star}_{\text{arm}-bc} + i^{\star}_{\text{arm}-ca}\right) \tag{3}$$

the following relationship for the converter arm current references is obtained:

$$\begin{bmatrix} i^{\star}_{\text{arm}-ab} \\ i^{\star}_{\text{arm}-bc} \\ i^{\star}_{\text{arm}-ca} \end{bmatrix} = \frac{1}{3}\begin{bmatrix} 1 & -1 & 0 \\ 0 & 1 & -1 \\ -1 & 0 & 1 \end{bmatrix}\begin{bmatrix} i^{\star}_a \\ i^{\star}_b \\ i^{\star}_c \end{bmatrix} + \begin{bmatrix} 1 \\ 1 \\ 1 \end{bmatrix} i^{\star}_{\text{circ}}. \tag{4}$$

Note that the previous definitions (3) and (4) guarantee that the grid currents are not affected by the circulating current. However, the circulating current affects the instantaneous capacitor voltages, thus providing a degree of freedom to achieve cluster (interphase) balancing [18], [21], among other objectives [19], [20].

Applying circuit analysis, and using (4), the instantaneous phase-arm converter voltage references in (2) can be alternatively expressed as follows:

$$\begin{aligned} \begin{bmatrix} v^{\star}_{ab} \\ v^{\star}_{bc} \\ v^{\star}_{ca} \end{bmatrix} &= \frac{1}{3}\begin{bmatrix} 1 & -1 & 0 \\ 0 & 1 & -1 \\ -1 & 0 & 1 \end{bmatrix}\left(L_{\text{eq}}\frac{d}{dt}\begin{bmatrix} i^{\star}_a \\ i^{\star}_b \\ i^{\star}_c \end{bmatrix} + R_{\text{eq}}\begin{bmatrix} i^{\star}_a \\ i^{\star}_b \\ i^{\star}_c \end{bmatrix}\right) \\ &\quad + \begin{bmatrix} e_{ab} \\ e_{bc} \\ e_{ca} \end{bmatrix} + \begin{bmatrix} 1 \\ 1 \\ 1 \end{bmatrix}\left(L_{\text{arm}}\frac{di^{\star}_{\text{circ}}}{dt} + R_{\text{arm}} i^{\star}_{\text{circ}}\right) \end{aligned} \tag{5}$$

where $R_{\text{eq}} = 3R + R_{\text{arm}}$ and $L_{\text{eq}} = 3L + L_{\text{arm}}$ represent the equivalent arm resistance and inductance, respectively, and e_{ab}, e_{bc}, and e_{ca} refer to the line-to-line PCC voltages.

C. Operational Limit of LC-StatComs in Inductive Mode

Operation of LC-StatComs based on CHB converters is limited by the fact that the cluster voltage reference $v^{\star}_{\Sigma-x}$ has to be higher than the ac-side voltage reference $v^{\star}_x$, i.e., $|v^{\star}_x| \leq v^{\star}_{\Sigma-x}$; otherwise, the corresponding modulating signal reference $\delta^{\star}_x$ saturates according to (2), i.e., $|\delta^{\star}_x| \geq 1$.

The aforementioned operational limit is analyzed here neglecting losses, and without considering circulating current injection, i.e., $i^{\star}_{\text{circ}} = 0$ in (4) and (5). These effects will be considered in the next section.

According to the converter dynamics, the cluster voltage references fulfill the following expression [24]:

$$v^{\star}_{\Sigma-x} C_{\text{arm}} \frac{dv^{\star}_{\Sigma-x}}{dt} = -v^{\star}_x i^{\star}_{\text{arm}-x} \tag{6}$$

where $C_{\text{arm}} = C/n$ represents the equivalent arm capacitance.

Using (4) and (5), and considering an ideal sinusoidal grid voltage and a sinusoidal injected current reference, i.e.,

$$\begin{aligned} e_x &= \hat{E}_L \cos(\omega t + \phi_x) \\ i^{\star}_{\text{arm}-x} &= \hat{I}^{\star}_{\text{arm}} \cos(\omega t + \varphi^{\star} + \phi_x) \end{aligned} \tag{7}$$

with $\phi_x \in \{0,\ -2\pi/3,\ 2\pi/3\}$ as the phase-shift among phases, the cluster voltage reference $v^{\star}_{\Sigma-x}$ can be analytically calculated from (6) as [2], [24], [29]

$$v^{\star}_{\Sigma-x} = \sqrt{(nV_{\text{UB}})^2 - \frac{\hat{V}^{\star}\hat{I}^{\star}_{\text{arm}}}{2\omega C_{\text{arm}}}\left(1 + \sin(2\omega t + \varphi^{\star} + 2\phi_x)\right)}. \tag{8}$$

Parameters $\hat{E}_L$ and ω stand for the amplitude of the line-to-line PCC voltages and the grid angular frequency, respectively. Parameters $\hat{I}^{\star}_{\text{arm}}$ and $\varphi^{\star}$ are the amplitude and phase of the differential arm current references. Ideally, without losses, phase shift $\varphi^{\star}$ is $\pi/2$ rad in inductive mode and $-\pi/2$ rad in capacitive mode (according to the convention of currents defined in Fig. 1). Parameter $\hat{V}^{\star}$ represents the amplitude of the ac-side voltage reference $v^{\star}_x$, and V_{UB} is the upper bound voltage, which is a prescribed constant value chosen to ensure safe circuit operation.

It is important to highlight that (8) ensures that the cluster voltage references $v^{\star}_{\Sigma-x}$ have a maximum at nV_{UB} [i.e., the maximum occurs when $\sin(2\omega t + \varphi^{\star} + 2\phi_x) = -1$ in (8)], and this maximum does not depend on the current amplitude reference $\hat{I}^{\star}_{\text{arm}}$ [2]. Nonetheless, the minimum in $v^{\star}_{\Sigma-x}$ does depend on $\hat{I}^{\star}_{\text{arm}}$, i.e., the higher the $\hat{I}^{\star}_{\text{arm}}$, the lower the minimum. In the capacitive mode, the cluster voltage reference $v^{\star}_{\Sigma-x}$ given by (8) is in phase alignment with the ac-side voltage reference $v^{\star}_x$; thus, large cluster voltage oscillations do not create any overmodulation issue. On the contrary, in the inductive mode, the oscillations are in counterphase, and therefore, the operation is limited, i.e., there could be periods of time where $|v^{\star}_x| \geq v^{\star}_{\Sigma-x}$, and hence, $|\delta^{\star}_x| \geq 1$ according to (2), which cannot be physically implemented [2], [15]. This limited operating range in the inductive region is defined in condition (9), which relates the minimum cluster voltage reference (left-hand side) with the amplitude $\hat{V}^{\star}$ of the ac-side voltage reference (right-hand side) during inductive operation. If the following condition is met, the LC-StatCom can provide the required inductive power

$$\sqrt{(nV_{\text{UB}})^2 - \frac{\left(\hat{E}_L - \omega L_{\text{eq}}\hat{I}^{\star}_{\text{arm}}\right)\hat{I}^{\star}_{\text{arm}}}{\omega C_{\text{arm}}}} \geq \left(\hat{E}_L - \omega L_{\text{eq}}\hat{I}^{\star}_{\text{arm}}\right). \tag{9}$$

In order to illustrate the previous limit, Fig. 2 shows reference waveforms of an LC-StatCom when an abrupt transient from full capacitive power to full inductive power occurs at $t = 0.05$ s. It can be observed that during some time periods in the inductive region, the required ac-side voltage reference $v^{\star}_x$ to provide the desired current $\hat{I}^{\star}_{\text{arm}}$ is higher than the required cluster voltage reference $v^{\star}_{\Sigma-x}$, i.e., $|v^{\star}_x| \geq v^{\star}_{\Sigma-x}$. In Fig. 2, these periods of time are shaded in light blue.

The next section deals with the calculation of a circulating current reference that shapes the cluster voltage references in such a way that they are always larger than the ac-side voltage references.

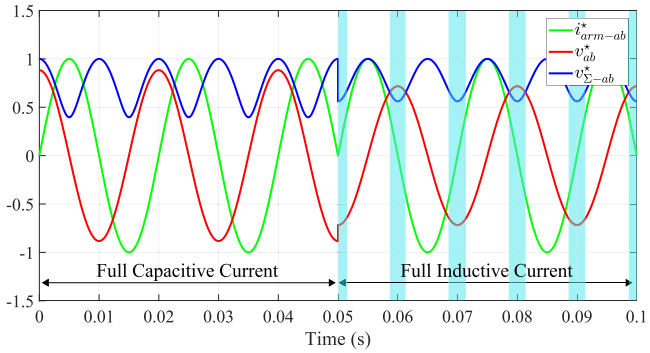

Fig. 2. Main reference signals in an LC-StatCom without circulating current injection. The blue waveform is the per unit cluster voltage reference, where the base voltage is $nV_{\rm UB}$. The green waveform is the per unit arm current reference, where the base current is $\hat{I}^\star_{\rm arm}$ at the rated power.

III. Cluster Voltage Shaping Method Using Third-Harmonic Circulating Current

This section describes a circulating current injection method to allow the LC-StatCom to operate at full range in the inductive mode. First, a case without losses is considered to facilitate the explanation of the proposed method, and then, the effect of losses is evaluated. Obviously, circulating current is only injected during the inductive mode and when condition (9) is not met, i.e., when the minimum cluster voltage references are lower than the amplitude of the ac-side voltage references.

Thus, the purpose of injecting the circulating current is to increase the value of the cluster voltage minimums. A third-harmonic circulating current reference $i^\star_{\rm circ}$ is considered, since the capacitor voltage oscillation has a frequency twice that of the grid voltage. Consequently, each cluster voltage has two minimums in a grid period, and then, along the grid period, there are six minimums due to the three phase arms (according to the 120° phase shift among phases). Thus, the circulating current needs to have a frequency that is three times that of the grid. Consequently, the arm current references $i^\star_{{\rm arm}-x}$ in the inductive mode in (7) are modified accordingly as

$$i^\star_{{\rm arm}-x} = -\hat{I}^\star_{\rm arm}\sin\left(\omega t+\phi_x\right)+\hat{I}^\star_{\rm circ}\sin\left(3\omega t\right) \tag{10}$$

where $\hat{I}^\star_{\rm circ}$ is the magnitude of the circulating current reference.

The proposed circulating current is a pure third harmonic. Any other circulating current with higher harmonics would require an increase in the converter bandwidth response. Moreover, higher harmonics in the circulating current will create larger voltage drops across the arm impedance that will appear at the ac-side voltage references $v^\star_x$ according to (5).

The ac-side converter voltage references $v^\star_x$ considering the third-harmonic circulating current can be calculated by substituting (10) into (4) and (5). The injection of the third-harmonic circulating current shapes the capacitor voltages. Then, the shaped cluster voltage references $v^\star_{\Sigma-x}$ can be calculated by solving the differential equation in (6) considering (10), i.e.,

$$v^\star_{\Sigma-x} = \sqrt{\left(v^\star_{\Sigma-x}(0)\right)^2-\frac{2}{C_{\rm arm}}\int v^\star_x i^\star_{{\rm arm}-x}dt} \tag{11}$$

for $x\in\{ab,\ bc,\ ca\}$, and where $v^\star_{\Sigma-x}(0)$ is the initial condition. Note that the integrator operator in (11) can be solved analytically since all the terms are sinusoidal.

Therefore, assuming no losses, the shaped cluster voltage reference for phase arm ab $v^\star_{\Sigma-ab}$ is as follows:

$$\begin{aligned} v^{\star 2}_{\Sigma-ab} = {} & V^{\star 2}_0-\frac{\hat{V}^\star\hat{I}^\star_{\rm arm}}{2\omega C_{\rm arm}}\cos\left(2\omega t\right) \\ & +\frac{\hat{V}^\star+3\omega L_{\rm arm}\hat{I}^\star_{\rm arm}}{2\omega C_{\rm arm}}\hat{I}^\star_{\rm circ}\cos\left(2\omega t\right) \\ & +\frac{\hat{V}^\star-3\omega L_{\rm arm}\hat{I}^\star_{\rm arm}}{4\omega C_{\rm arm}}\hat{I}^\star_{\rm circ}\cos\left(4\omega t\right) \\ & +\frac{L_{\rm arm}}{2C_{\rm arm}}\hat{I}^{\star 2}_{\rm circ}\cos\left(6\omega t\right). \end{aligned} \tag{12}$$

Similar expressions can be readily written for the other converter arms. Variable $V^{\star 2}_0$ is the dc component of the square cluster voltage references. Comparing (12) with (8), the circulating current injection adds three extra harmonic components, namely, a second (2ω) negative-sequence harmonic, a fourth (4ω) positive-sequence harmonic, and a sixth (6ω) harmonic that is common in the three cluster voltages. It is important to note that the circulating current phase angle chosen in (10) yields an extra second harmonic in (12) that is in counterphase with the original second harmonic [14]. This circulating current phase angle ensures that the compensation action by the circulating current is symmetrical. The value of the shaped cluster voltage $v^\star_{\Sigma-ab}$, according to (12), at time instants $2\omega t=0+2k\pi$ with k as an integer number, is denoted in the following as V_{SCm}, and it has to be higher than the ac-side converter voltage reference $v^\star_x$. Any loss of symmetry, due to a different circulating current phase, will shift the time instant in which V_{SCm} occurs and, consequently, will involve a larger circulating current.

Once the shaped cluster voltage references $v^\star_{\Sigma-x}$ and ac-side converter voltage references $v^\star_x$ are derived, the modulating signal references $\delta^\star_x$ are calculated according to (2).

In the following, the shaped cluster voltage $v^\star_{\Sigma-ab}$, according to (12), at time instants $2\omega t=\pi+2k\pi$, is denoted as V_{SCM}, and it will be used in the derivation of the circulating current amplitude.

It is important to highlight that this reference design criterion stands in contrast with that commonly adopted in the conventional StatCom applications, where the capacitor voltages are regarded as constant.

A. Optimal Amplitude of Third-Harmonic Circulating Current: The Lossless Case

The amplitude of the proposed circulating current $\hat{I}^\star_{\rm circ}$ and the dc component of the square cluster voltage references $V^{\star 2}_0$ represent two degrees of freedom to shape the cluster voltage references $v^\star_{\Sigma-x}$ [see (12)]. In this subsection, a constrained optimization problem is formulated, which aims to minimize $\hat{I}^\star_{\rm circ}$ while satisfying that: 1) V_{SCm} is higher than the ac-side converter voltage reference $v^\star_x$, and 2) V_{SCM} is lower than a prescribed maximum value $nV_{\rm UB}$. Obviously, minimizing the

circulating current $\hat{I}^{\star}_{\text{circ}}$ results in minimizing the rms arm current, which is related to conduction losses in the arms.

Evaluating (12) at time instants $2\omega t = 0 + 2k\pi$, V^2_{SCm} corresponds to

$$V^2_{SCm} = \left(V_0^{\star 2} - \frac{\hat{V}^{\star}\hat{I}^{\star}_{\text{arm}}}{2\omega C_{\text{arm}}}\right) + \frac{3\left(\hat{V}^{\star} + \omega L_{\text{arm}}\hat{I}^{\star}_{\text{arm}}\right)}{4\omega C_{\text{arm}}}\hat{I}^{\star}_{\text{circ}} + \frac{L_{\text{arm}}}{2C_{\text{arm}}}\hat{I}^{\star 2}_{\text{circ}} \tag{13}$$

which defines a second-order equation in terms of the unknown amplitude of the circulating current reference $\hat{I}^{\star}_{\text{circ}}$. Note that the independent term corresponds to the original minimum, i.e., when no circulating current is injected, and that the rest of the terms are strictly positive and, therefore, help to raise the original minimum. V_{SCm} has to be always larger than or equal to the shaped ac-side voltage reference $v^{\star}_x$, i.e., for the phase arm ab

$$V_{SCm} \geq h v^{\star}_{ab}\,(\omega t = 0 + k\pi) \tag{14}$$

with the parameter $h \geq 1$. Note that h models a desired slack in the condition (14). Note also that $h > 1$ implies that the shaped modulating signal references $\delta^{\star}_x$ are strictly smaller than 1, according to (2). Thus, substituting the value of V_{SCm} given by (13), we can rewrite (14) as

$$\left(-\frac{L_{\text{arm}}}{2C_{\text{arm}}} + (h3\omega L_{\text{arm}})^2\right)\hat{I}^{\star 2}_{\text{circ}} + \left(-\frac{3\left(\hat{V}^{\star} + \omega L_{\text{arm}}\hat{I}^{\star}_{\text{arm}}\right)}{4\omega C_{\text{arm}}} + h^2 6\omega L_{\text{arm}}\hat{V}^{\star}\right)\hat{I}^{\star}_{\text{circ}} + \left(\frac{\hat{V}^{\star}\hat{I}^{\star}_{\text{arm}}}{2\omega C_{\text{arm}}} + h^2\hat{V}^{\star 2}\right) \leq V_0^{\star 2} \tag{15}$$

which defines an admissible area in the $(\hat{I}^{\star}_{\text{circ}},\ V_0^{\star 2})$ plane.

Similarly, the V^2_{SCM} value is derived using (12) particularized at $2\omega t = \pi + 2k\pi$ and corresponds to

$$V^2_{SCM} = \left(V_0^{\star 2} + \frac{\hat{V}^{\star}\hat{I}^{\star}_{\text{arm}}}{2\omega C_{\text{arm}}}\right) - \frac{\hat{V}^{\star} + 9\omega L_{\text{arm}}\hat{I}^{\star}_{\text{arm}}}{4\omega C_{\text{arm}}}\hat{I}^{\star}_{\text{circ}} + - \frac{L_{\text{arm}}}{2C_{\text{arm}}}\hat{I}^{\star 2}_{\text{circ}} \tag{16}$$

which again is a second-order equation in terms of $\hat{I}^{\star}_{\text{circ}}$. Note that the independent term corresponds to the original maximum value, i.e., when no circulating current is injected, and that the rest of the terms are strictly negative and, therefore, help to lower the original maximum. The V_{SCM} has to be always lower than or equal to the prescribed upper bound voltage nV_{UB}, i.e.,

$$V_{SCM} \leq nV_{\text{UB}}. \tag{17}$$

Considering that the circulating current $\hat{I}^{\star}_{\text{circ}}$ is desired to be considerably smaller than $\hat{I}^{\star}_{\text{arm}}$, and taking into account that the coefficients of the second-order terms of (13) and (16) are smaller than the first-order terms, the second-order terms of (13) and (16) can be neglected. Therefore, (14) and (17) can be approximated as a pair of two linear constraints.

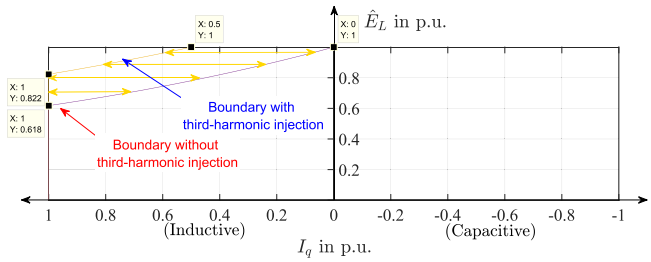

Fig. 3. $\hat{E}_L$–I_q characteristic of the LC-StatCom with and without the proposed third-harmonic circulating current injection method. The reactive current I_q has been defined as $I_q = \hat{I}^{\star}_{\text{arm}}\sin(\varphi^{\star})$.

Thus, the problem of minimizing the circulating current under the previous constraints can be modeled as the next linear programming problem

$$\begin{aligned} &\text{Minimize} \quad \hat{I}^{\star}_{\text{circ}} \\ &\text{subject to} \quad A_c \begin{bmatrix} \hat{I}^{\star}_{\text{circ}} \\ V_0^{\star 2} \end{bmatrix} \geq b_c \\ &\text{and} \quad \begin{bmatrix} \hat{I}^{\star}_{\text{circ}} \\ V_0^{\star 2} \end{bmatrix} \geq \begin{bmatrix} 0 \\ 0 \end{bmatrix} \end{aligned} \tag{18}$$

where the matrix A_c, which groups the constraint coefficients, and the vector b_c, which groups the independent terms in the constraints, correspond to

$$A_c = \begin{bmatrix} \frac{3\left(\hat{V}^{\star} + \omega L_{\text{arm}}\hat{I}^{\star}_{\text{arm}}\right)}{4\omega C_{\text{arm}}} - 6h^2\omega L_{\text{arm}}\hat{V}^{\star} & 1 \\ \frac{\hat{V}^{\star} + 9\omega L_{\text{arm}}\hat{I}^{\star}_{\text{arm}}}{4\omega C_{\text{arm}}} & -1 \end{bmatrix} \tag{19}$$

$$b_c = \begin{bmatrix} \left(h\hat{V}^{\star}\right)^2 + \frac{\hat{V}^{\star}\hat{I}^{\star}_{\text{arm}}}{2\omega C_{\text{arm}}} \\ -\left(nV_{\text{UB}}\right)^2 + \frac{\hat{V}^{\star}\hat{I}^{\star}_{\text{arm}}}{2\omega C_{\text{arm}}} \end{bmatrix}. \tag{20}$$

Note that A_c and b_c define a set of feasible solutions in the $(\hat{I}^{\star}_{\text{circ}},\ V_0^{\star 2})$ plane.

The solution of the linear programming problem (18), namely, the optimal point $(\hat{I}^{\star\text{opt}}_{\text{circ}},\ V_0^{\star 2\text{opt}})$, corresponds to

$$\begin{bmatrix} \hat{I}^{\star\text{opt}}_{\text{circ}} \\ V_0^{\star 2\text{opt}} \end{bmatrix} = A_c^{-1} b_c. \tag{21}$$

Therefore, according to (21), the optimal circulating current $\hat{I}^{\star\text{opt}}_{\text{circ}}$ corresponds to

$$\hat{I}^{\star\text{opt}}_{\text{circ}} = \frac{\hat{V}^{\star}\hat{I}^{\star}_{\text{arm}} - \omega C_{\text{arm}}\left[\left(nV_{\text{UB}}\right)^2 - \left(h\hat{V}^{\star}\right)^2\right]}{\hat{V}^{\star} + 3\omega L_{\text{arm}}\hat{I}^{\star}_{\text{arm}} - 6h^2\omega^2 C_{\text{arm}} L_{\text{arm}}\hat{V}^{\star}} \tag{22}$$

where it can be noted that the greater the term $(nV_{\text{UB}})^2 - (h\hat{V}^{\star})^2$ is—which represents the quadratic difference between the maximum and the minimum allowable shaped cluster voltages—the smaller the circulating current $\hat{I}^{\star\text{opt}}_{\text{circ}}$ has to be to achieve full-range inductive operation.

Fig. 3, which has been obtained according to [2] and [15], depicts the enhancement of inductive range in an ideal case, i.e., when the filtering impedances are neglected, the slack

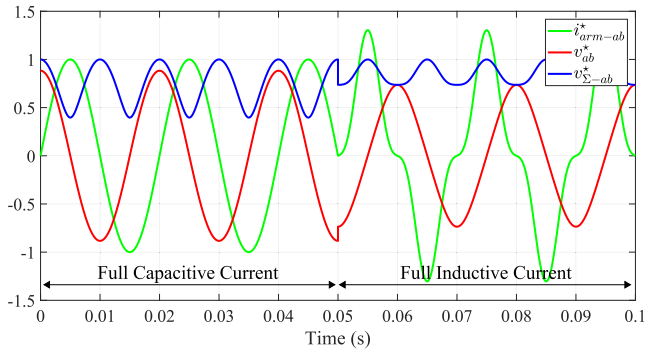

Fig. 4. Main reference signals in an LC-StatCom with the proposed circulating current injection. The blue waveform is the per unit cluster voltage reference, where the base voltage is nV_{UB}. The green waveform is the per unit arm current reference, where the base current is $\hat{I}^{\star}_{\text{arm}}$ at the rated power. Slack parameter value is $h = 1$.

variable h is 1, and with the assumption that the capacitor voltage oscillation reaches its theoretical 100% limit at rated condition. Fig. 3 shows the operating limits when no circulating current is injected (shown in the figure by means of an arrow and a comment in red), and the operating limit when the optimal circulating current is injected (shown in the figure by means of an arrow and a comment in blue).

A more realistic case, that is, when the capacitor voltage oscillation is above 60% of its dc values, is illustrated in Fig. 4, showing the current and voltage references that an LC-StatCom has to follow when the operation state changes from capacitive to inductive power at $t = 0.05$ s. Note that, unlike in Fig. 2 when no circulating current was injected, in Fig. 4, the LC-StatCom can operate at full inductive power without saturating the modulating signal.

Note that (10) only considers a positive-sequence reactive power compensation. If any other harmonic component is required, e.g., for negative-sequence reactive power compensation, the procedure to enhance the inductive operation mode should be modified to take into account the new phase and magnitude of the capacitor voltages oscillation.

B. Optimal Amplitude of Third-Harmonic Circulating Current: The Losses Case

This subsection addresses the effect of power losses on the phase and amplitude of the optimal injected third-harmonic circulating current. The losses modify V^2_{SCm} and V^2_{SCM} in (13) and (16), respectively. Consequently, the optimal point in (21) has to be calculated accordingly.

When losses are considered, the phase shift $\varphi^{\star}$ between the grid current references $i^{\star}_a$, $i^{\star}_b$, and $i^{\star}_c$, and the PCC voltages e_a, e_b, and e_c is not purely reactive [24], namely

$$\varphi^{\star} = \pm\left(\pi/2 + \alpha^{\star}\right) \tag{23}$$

where the positive losses compensation angle $\alpha^{\star} \geq 0$ guarantees zero dc power component in the arms during steady state [24], i.e.,

$$\frac{3}{2}\left(\hat{E}_L \hat{I}^{\star}_{\text{arm}} \sin\left(\alpha^{\star}\right) - R_{eq}\hat{I}^{\star 2}_{\text{arm}} - R_{\text{arm}}\hat{I}^{\star 2}_{\text{circ}}\right) = 0. \tag{24}$$

Otherwise, the accumulated energy in the capacitors will increase or decrease during a period. According to (24), the losses compensation angle $\alpha^{\star}$ corresponds to

$$\alpha^{\star} = \arcsin\left(\frac{R_{eq}\hat{I}^{\star 2}_{\text{arm}} + R_{\text{arm}}\hat{I}^{\star 2}_{\text{circ}}}{\hat{E}_L \hat{I}^{\star}_{\text{arm}}}\right) \tag{25}$$

which is determined by the losses in the converter at the operating point. Obviously, the circuit is not purely reactive when $R_{\text{arm}} \neq 0$ or $R \neq 0$, and the phase shift $\alpha^{\star}$ takes into account the relationship between the active power absorbed from the grid, that compensates for the losses, and the apparent power drawn from the grid.

Note that $R_{\text{eq}}\hat{I}^{\star 2}_{\text{arm}} \gg R_{\text{arm}}\hat{I}^{\star 2}_{\text{circ}}$ because: 1) R_{arm} is usually considerably smaller than $R_{\text{eq}} = 3R + R_{\text{arm}}$; and 2) $\hat{I}^{\star}_{\text{circ}}$ is designed to be considerably smaller than $\hat{I}^{\star}_{\text{arm}}$ in order to have a reasonable level of losses. Thus, (25) can be approximated by

$$\alpha^{\star} \approx \arcsin\left(\frac{R_{\text{eq}}\hat{I}^{\star}_{\text{arm}}}{\hat{E}_L}\right) \tag{26}$$

which facilitates writing V^2_{SCm} and V^2_{SCM} expressions as second-order equations in terms of $\hat{I}^{\star}_{\text{circ}}$.

Consequently, the injected circulating current has to take into account this phase shift. Hence, the arm current references $i^{\star}_{\text{arm}-x}$ in (10) are modified as

$$i^{\star}_{\text{arm}-x} = -\hat{I}^{\star}_{\text{arm}} \sin\left(\omega t + \alpha^{\star} + \phi_x\right) + \hat{I}^{\star}_{\text{circ}} \sin\left(3\omega t + 3\alpha^{\star}\right). \tag{27}$$

The ac-side converter voltage references $v^{\star}_x$ considering the third-harmonic circulating current and the losses can be calculated by substituting (27) into (4) and (5). Subsequently, the shaped cluster voltage references $v^{\star}_{\Sigma-x}$ can be calculated by solving (11). Hence, the shaped cluster voltage reference in (12) is modified accordingly as

$$\begin{aligned} v^{\star 2}_{\Sigma-ab} = {} & V^{\star 2}_0 - A_0 \cos\left(2\omega t - \psi_0\right) \\ & + A_1 \hat{I}^{\star}_{\text{circ}} \cos\left(2\omega t - \psi_1\right) \\ & + A_2 \hat{I}^{\star}_{\text{circ}} \cos\left(4\omega t - \psi_2\right) \\ & + A_3 \hat{I}^{\star 2}_{\text{circ}} \cos\left(6\omega t - \psi_3\right) \end{aligned} \tag{28}$$

where the amplitude A_i and phase ψ_i are defined as

$$A_i = \sqrt{\alpha_i^2 + \beta_i^2},\ \psi_i = \arctan 2\left(\beta_i,\ \alpha_i\right) \tag{29}$$

where coefficients α_i and β_i are shown in Table II in the Appendix. As it can be observed, $\beta_i = 0\ \forall i$ in the lossless case, resulting in $A_i = \alpha_i$ and $\psi_i = 0$, and then, (28) is equivalent to (12).

V_{SCm} associated with (28) can be analytically calculated by substituting $2\omega t = \psi_0 + 2k\pi$. Similarly, V_{SCM} for the losses case is calculated by evaluating (28) at $2\omega t = \pi + \psi_0 + 2k\pi$.

Similar to the lossless case, again imposing constraints (14) and (17), a linear programming problem as in (18) can be formulated. Note that the shaped ac-side voltage reference $v^{\star}_x$, which is needed in the V_{SCm} constraint (14), is modified for the

TABLE I
EXPERIMENTAL SYSTEM PARAMETERS

Parameter		Value
PCC Voltage Nominal Amplitude, $\hat{E}_L$		$30\sqrt{2}\sqrt{3}$ V (1 p.u.)
Nominal Power, S		670 VA (1 p.u.)
Grid Angular Frequency, ω_g		20π rad/s
Individual Switch Switching Frequency, f_{sw}		5 kHz
Upper Bound Voltage, V_{UB}		92 V
Slack Variable, h		1.05
Capacitance per H-Bridge, C		1.10 mF
Filter Inductances,	L	5 mH (0.079 p.u.)
	L_{arm}	5 mH (0.079 p.u.)
Parasitic Resistances,	R	150 mΩ (0.038 p.u.)
	R_{arm}	150 mΩ (0.038 p.u.)

losses case, in particular for the phase arm ab, as follows:

$$v^{\star}_{ab} = A_4 \cos(\omega t - \psi_4) + \hat{I}^{\star}_{\text{circ}} A_5 \cos(3\omega t - \psi_5). \quad (30)$$

The matrix A_c and vector b_c for the losses case become

$$A_c = \begin{bmatrix} a_{c11} & 1 \\ a_{c21} & -1 \end{bmatrix} \quad (31)$$

$$b_c = \begin{bmatrix} (hA_4 \cos(\psi_0/2 - \psi_4))^2 + A_0 \\ -(nV_{UB})^2 + A_0 \end{bmatrix} \quad (32)$$

where the matrix A_c coefficients are

$$a_{c11} = A_1 \cos(\psi_0 - \psi_1) + A_2 \cos(2\psi_0 - \psi_2) + \\ - 2h^2 A_4 A_5 \cos(\psi_0/2 - \psi_4) \cos(3\psi_0/2 - \psi_5) \quad (33)$$

$$a_{c21} = A_1 \cos(\psi_0 - \psi_1) - A_2 \cos(2\psi_0 - \psi_2). \quad (34)$$

Again, the solution to this linear programming problem can be found as in (21), i.e.,

$$\begin{bmatrix} \hat{I}^{\star\text{opt}}_{\text{circ}} \\ V_0^{\star 2\text{opt}} \end{bmatrix} = A_c^{-1} b_c. \quad (35)$$

Then, according to (35), the optimal circulating current $\hat{I}^{\star\text{opt}}_{\text{circ}}$ corresponds to

$$\hat{I}^{\star\text{opt}}_{\text{circ}} = \\ \frac{A_0 - (1/2)\left[(nV_{UB})^2 - (hA_4 \cos(\psi_0/2 - \psi_4))^2\right]}{A_1 \cos(\psi_0 - \psi_1) - h^2 A_4 A_5 \cos(\psi_0/2 - \psi_4) \cos(3\psi_0/2 - \psi_5)}. \quad (36)$$

However, having an explicit expression of ($\hat{I}^{\star\text{opt}}_{\text{circ}}$, $V_0^{\star 2\text{opt}}$) may not be needed because most modern digital control devices are able to implement the matrix inversion operation.

IV. POWER LOSS AND CURRENT STRESS ANALYSIS

With the purpose of providing a comprehensive assessment of the proposed third-harmonic injection method, this section quantifies the increase in power loss and semiconductors' current stress when the converter operates with the proposed circulating current injection.

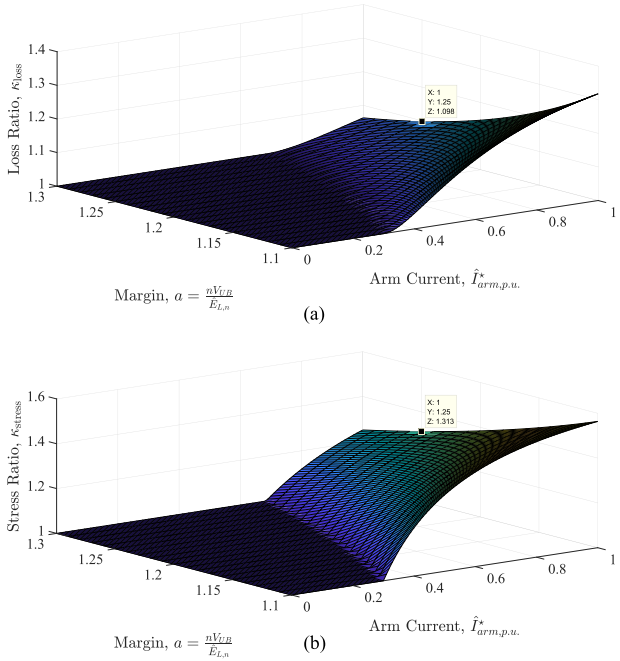

Fig. 5. (a) Loss ratio and (b) stress ratio due to the proposed third-harmonic circulating current injection.

The conduction loss in one phase arm of the StatCom can be modeled as follows [12]:

$$P_{R_{\text{arm}}} = R_{\text{arm}} \left(\frac{1}{T_g} \int_0^{T_g} i^2_{\text{arm}} dt \right) \quad (37)$$

where $T_g = 2\pi/\omega_g$ is the fundamental period. Using (27) yields

$$P_{R_{\text{arm}}} = \frac{R_{\text{arm}}}{2} \left(\hat{I}^{\star 2}_{\text{arm}} + \hat{I}^{\star 2}_{\text{circ}} \right). \quad (38)$$

Thus, the increase in conduction loss can be quantified by defining the ratio κ_{loss} between the conduction loss when third-harmonic zero-sequence injection is applied and the conduction loss without third-harmonic injection, i.e.,

$$\kappa_{\text{loss}} = \frac{\frac{R_{\text{arm}}}{2}\left(\hat{I}^{\star 2}_{\text{arm}} + \hat{I}^{\star 2}_{\text{circ}} \right)}{\frac{R_{\text{arm}}}{2} \hat{I}^{\star 2}_{\text{arm}}} = 1 + \left(\frac{\hat{I}^{\star}_{\text{circ}}}{\hat{I}^{\star}_{\text{arm}}} \right)^2. \quad (39)$$

The current stress is also an important indicator that is studied next. The increase in current stress can be quantified by defining the ratio κ_{stress} between the peak arm current when third-harmonic zero-sequence injection is applied and the peak arm current without third-harmonic injection, i.e.,

$$\kappa_{\text{stress}} = \frac{\hat{I}^{\star}_{\text{arm}} + \hat{I}^{\star}_{\text{circ}}}{\hat{I}^{\star}_{\text{arm}}} = 1 + \frac{\hat{I}^{\star}_{\text{circ}}}{\hat{I}^{\star}_{\text{arm}}}. \quad (40)$$

Fig. 5 shows how the aforementioned ratios depend on the capacitance value and the required power value. Specifically, Fig. 5 depicts the loss and stress ratios for a range of $[10\%, 30\%]$ in the voltage margin $V_{\text{UB}}/\hat{E}_{L,n}$ and a range of $[0, 100\%]$ in the current magnitude $\hat{I}_{\text{arm}}$. $\hat{E}_{L,n}$ refers to the nominal grid voltage.

TABLE II
EXPRESSIONS FOR α_i AND β_i COEFFICIENTS

Symbol	Losses Case	Lossless Case
α_0	$\frac{1}{2\omega C_{arm}}\hat{I}^{\star}_{arm}\left(\hat{E}_L\cos(\alpha^{\star})-\omega L_{eq}\hat{I}^{\star}_{arm}\cos(2\alpha^{\star})-R_{eq}\hat{I}^{\star}_{arm}\sin(2\alpha^{\star})\right)$	$\frac{1}{2\omega C_{arm}}\hat{I}^{\star}_{arm}\left(\hat{E}_L-\omega L_{eq}\hat{I}^{\star}_{arm}\right)$
β_0	$-\frac{1}{2\omega C_{arm}}\hat{I}^{\star}_{arm}\left(\hat{E}_L\sin(\alpha^{\star})-\omega L_{eq}\hat{I}^{\star}_{arm}\sin(2\alpha^{\star})+R_{eq}\hat{I}^{\star}_{arm}\cos(2\alpha^{\star})\right)$	0
α_1	$\frac{1}{2\omega C_{arm}}\left(\hat{E}_L\cos(3\alpha^{\star})+3\omega L_{arm}\hat{I}^{\star}_{arm}\cos(2\alpha^{\star})-\omega L_{eq}\hat{I}^{\star}_{arm}\cos(2\alpha^{\star})+(R_{eq}+R_{arm})\hat{I}^{\star}_{arm}\sin(2\alpha^{\star})\right)$	$\frac{1}{2\omega C_{arm}}\left(\hat{E}_L-\omega L_{eq}\hat{I}^{\star}_{arm}+3\omega L_{arm}\hat{I}^{\star}_{arm}\right)$
β_1	$-\frac{1}{2\omega C_{arm}}\left(\hat{E}_L\sin(3\alpha^{\star})+3\omega L_{arm}\hat{I}^{\star}_{arm}\sin(2\alpha^{\star})-\omega L_{eq}\hat{I}^{\star}_{arm}\sin(2\alpha^{\star})-(R_{eq}+R_{arm})\hat{I}^{\star}_{arm}\cos(2\alpha^{\star})\right)$	0
α_2	$\frac{1}{4\omega C_{arm}}\left(\hat{E}_L\cos(3\alpha^{\star})-3\omega L_{arm}\hat{I}^{\star}_{arm}\cos(4\alpha^{\star})-\omega L_{eq}\hat{I}^{\star}_{arm}\cos(4\alpha^{\star})-(R_{eq}+R_{arm})\hat{I}^{\star}_{arm}\sin(4\alpha^{\star})\right)$	$\frac{1}{4\omega C_{arm}}\left(\hat{E}_L-\omega L_{eq}\hat{I}^{\star}_{arm}-3\omega L_{arm}\hat{I}^{\star}_{arm}\right)$
β_2	$-\frac{1}{4\omega C_{arm}}\left(\hat{E}_L\sin(3\alpha^{\star})-3\omega L_{arm}\hat{I}^{\star}_{arm}\sin(4\alpha^{\star})-\omega L_{eq}\hat{I}^{\star}_{arm}\sin(4\alpha^{\star})+(R_{eq}+R_{arm})\hat{I}^{\star}_{arm}\cos(4\alpha^{\star})\right)$	0
α_3	$\frac{1}{6\omega C_{arm}}\left(3\omega L_{arm}\cos(6\alpha^{\star})+R_{arm}\sin(6\alpha^{\star})\right)$	$\frac{L_{arm}}{2C_{arm}}$
β_3	$-\frac{1}{6\omega C_{arm}}\left(3\omega L_{arm}\sin(6\alpha^{\star})-R_{arm}\cos(6\alpha^{\star})\right)$	0
α_4	$\hat{E}_L-\omega L_{eq}\hat{I}^{\star}_{arm}\cos(\alpha^{\star})-R_{eq}\hat{I}^{\star}_{arm}\sin(\alpha^{\star})$	$\hat{E}_L-\omega L_{eq}\hat{I}^{\star}_{arm}$
β_4	$\omega L_{eq}\hat{I}^{\star}_{arm}\sin(\alpha^{\star})-R_{eq}\hat{I}^{\star}_{arm}\cos(\alpha^{\star})$	0
α_5	$3\omega L_{arm}\cos(3\alpha^{\star})+R_{arm}\sin(3\alpha^{\star})$	$3\omega L_{arm}$
β_5	$-3\omega L_{arm}\sin(3\alpha^{\star})+R_{arm}\cos(3\alpha^{\star})$	0

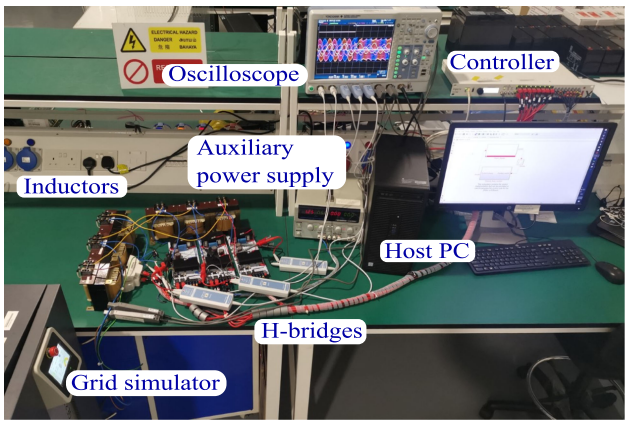

Fig. 6. Experimental setup.

V. EXPERIMENTAL RESULTS

This section presents experimental measurements that illustrate the compensated LC-StatCom behavior concerning its ability to provide full-range inductive operation, while fulfilling the design constraints (i.e., no saturation and operation in a safe range). First, the constructed prototype is described and its main parameters are defined. Then, experimental measurements are illustrated with the purpose of assessing the optimal third-harmonic circulating current injection method.

The experimental LC-StatCom prototype is connected to a 30-V grid, and it has a rated apparent power of 670 VA. The inductors have been sized to provide a rated voltage drop of approximately 10% between the converter ac-side voltage and the PCC voltage. This results in 33-Vrms line-to-neutral output voltage from the StatCom at 7.42 A rms. Table I provides the system parameters and Fig. 6 shows the experimental setup. The prototype has one submodule per phase. However, the proposed third-harmonic circulating current injection method has been tested by simulation in a high-power multilevel LC-StatCom with five submodules per arm, and the corresponding results are described in Section VI. Note that despite the fact that no extra hardware is needed, sizing and technology of switching components and dc-link capacitors could be affected by the injected circulating current due to increase in the arm current magnitude (roughly 33% in the presented experimental case).

The PCC voltage is provided by a GE&EL 15-kVA CINERGIA grid emulator. In the setup, three IMPERIX PEH2015 H-bridge converters are used to construct a three-level LC-StatCom with delta configuration, with a dc-link capacitor of 1.1 mF. The prescribed maximum voltage on each capacitor in the current system is $V_{\mathrm{UB}} = 92$ V. A slack parameter value $h = 1.05$ is used to guarantee that the modulating functions are not saturated during normal operation. The reference signals described in Sections II and III, together with the controller block, are implemented in a B-Box RCP 3.0 board from IMPERIX. The controller programmed here is based on that presented in [24], but adapted to the three-phase case with delta connection. Nonetheless, the same approach can be used with a conventional control as in [18].

The operation of the compensated LC-StatCom with the third-harmonic circulating current injection method is tested under an abrupt change in the imaginary power reference $q^{\star}$, from 100% rated power capacitive mode to 100% rated power inductive mode. Fig. 7 shows the ac-side pulsewidth modulation (PWM) converter voltages and the corresponding capacitor voltages for each phase arm. The voltages v_x are shaped by the capacitor voltages $v_{\Sigma-x}$, and this is a consequence of physical restraint $|v_x| \leq v_{\Sigma-x}$. Moreover, the voltage references have also been added to provide a better visualization. It can be observed that the LC-StatCom recovers its desired behavior very fast after the change that occurs in $t = 0.25$ s, and the compensated LC-StatCom has capability to inject the desired current in the entire power range. When the transient occurs at $t = 0.25$ s, saturation appears in phase arms bc and ca momentarily because there is not

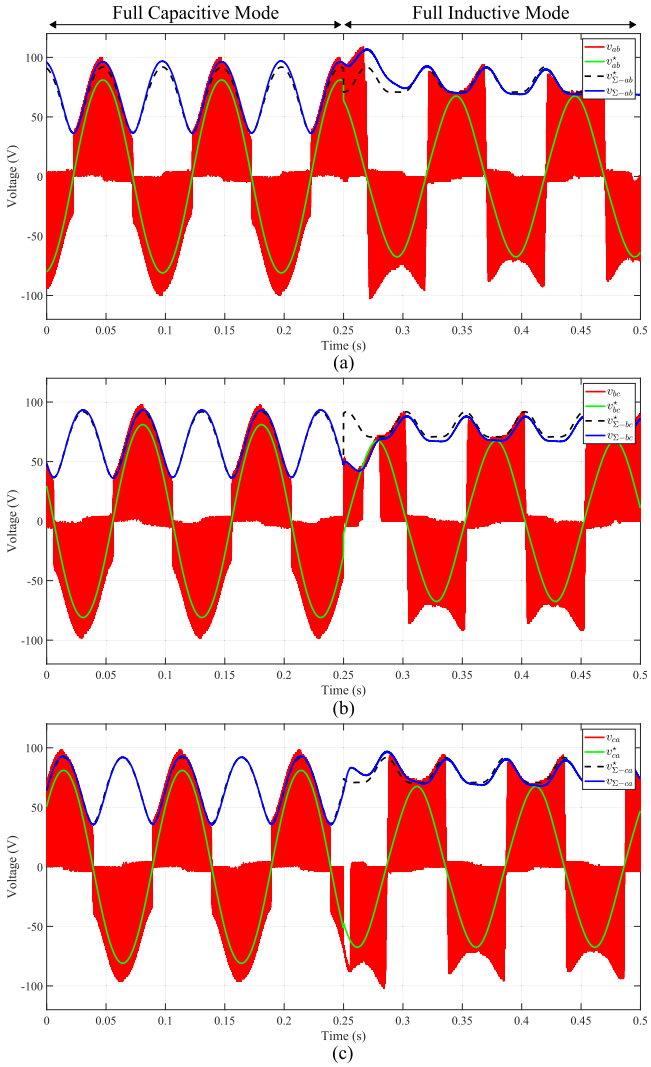

Fig. 7. Experimental waveforms of ac-side PWM converter voltages v_{ab}, v_{bc}, and v_{ca}, and cluster voltages $v_{\Sigma-ab}$, $v_{\Sigma-bc}$, and $v_{\Sigma-ca}$, during a sudden reactive power change from 100% rated power capacitive mode to 100% rated power inductive mode at $t = 0.25$ s. (a) Phase arm ab. (b) Phase arm bc. (c) Phase arm ca.

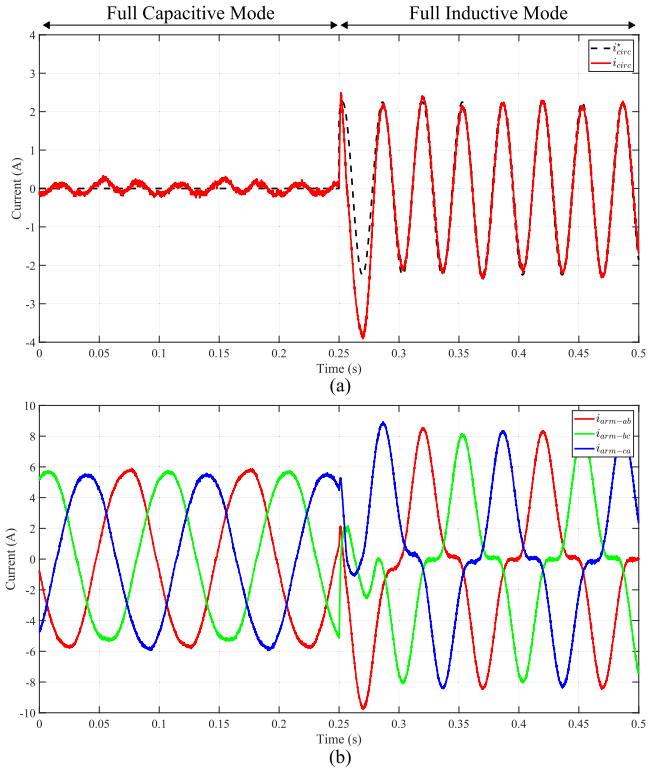

Fig. 8. Experimental waveforms of (a) circulating current i_{circ} and (b) arm currents $i_{\text{arm}-ab}$, $i_{\text{arm}-bc}$, and $i_{\text{arm}-ca}$, during a sudden reactive power change from 100% rated power capacitive mode to 100% rated power inductive mode at $t = 0.25$ s.

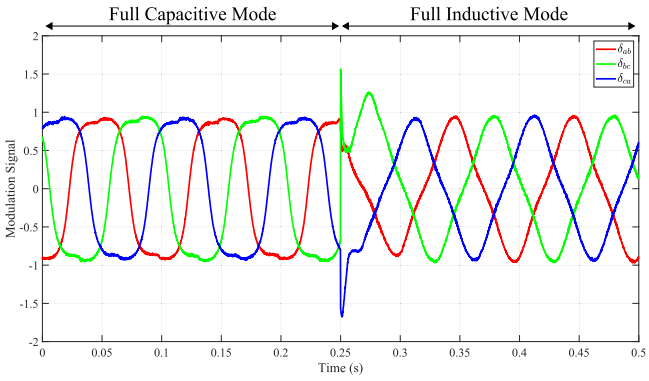

Fig. 9. Experimental waveforms of modulating signals δ_{ab}, δ_{bc}, and δ_{ca}, during a sudden reactive power change from 100% rated power capacitive mode to 100% rated power inductive mode at $t = 0.25$ s.

enough cluster voltage to provide the required ac-side voltage reference, i.e., $|v_x^\star| > v_{\Sigma-x}$. Also, it can be appreciated that due to the low capacitance used, the capacitor voltages present an oscillation (low-frequency ripple) above 50% of their dc values during capacitive operation [30]. Experimental results in Fig. 7 are in perfect agreement with the simulated reference signals shown in Fig. 4, thus corroborating the analytical derivations. The compensated LC-StatCom is able to maintain control of the capacitor voltages and the arm currents throughout the entire power range, even at 100% rated power in the inductive mode.

The circulating current i_{circ} and arm currents $i_{\text{arm}-ab}$, $i_{\text{arm}-bc}$, and $i_{\text{arm}-ca}$ are depicted in Fig. 8, while the modulating functions generated by the controller δ_{ab}, δ_{bc}, and δ_{ca} are shown in Fig. 9. Prior to $t = 0.25$ s, the circulating current is almost zero due to the balanced system operation, whereas from $t = 0.25$s, the optimal third-harmonic circulating current begins to be injected in order to suitably shape the cluster voltages. As a result, the modulating signals δ_x are in the range $[-1,\ 1]$ during steady state. It is important to note that the maximal value of modulating signal references is determined by the slack parameter h. It can be seen that the circulating current amplitude needed to allow full inductive operation represents approximately $1/3$ of the rated arm current amplitude. Therefore, the fact of injecting a third-harmonic circulating current implies, for the operating point presented in the above experiments, an approximately 10% increase in the conduction loss, and an increase of one third in the amplitude of the arm currents. The experimental recordings of increased losses and current stress are in close agreement

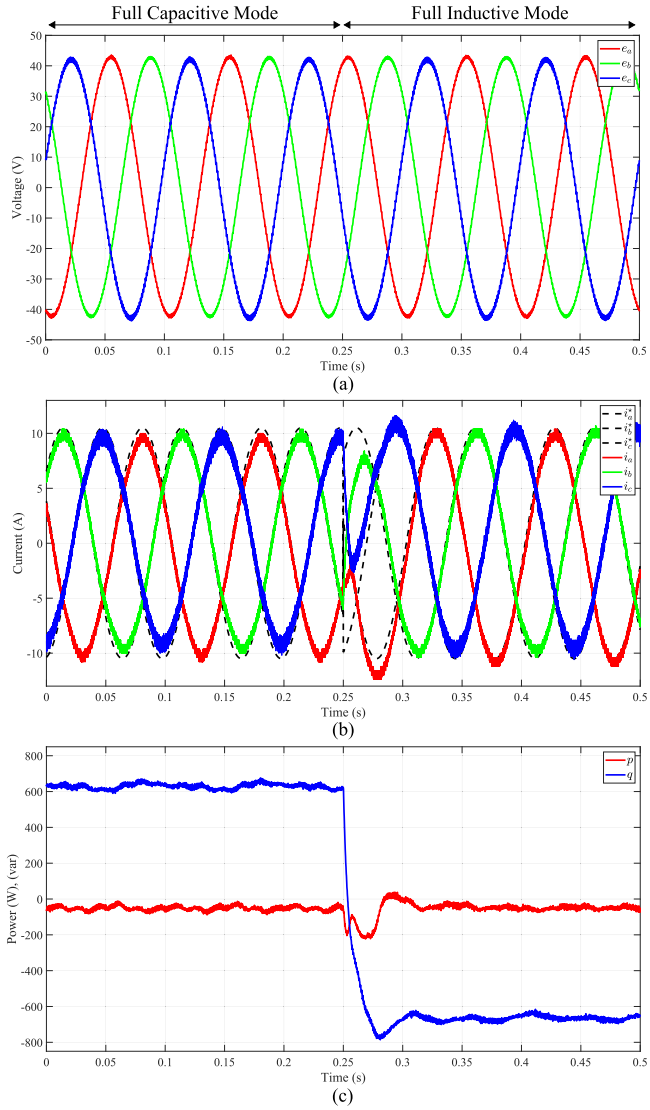

Fig. 10. Experimental waveforms (a) line-to-neutral PCC voltages e_a, e_b, and e_c, (b) grid currents i_a, i_b, and i_c, and (c) instantaneous powers p and q, during a sudden reactive power change from 100% rated power capacitive mode to 100% rated power inductive mode at $t = 0.25$ s.

with analytical predictions derived from (39) and (40), and the corresponding Fig. 5, i.e., $\kappa_{\text{loss}} \approx 1.11$ and $\kappa_{\text{stress}} \approx 1.33$.

Fig. 10 shows the grid currents i_a, i_b, and i_c and instantaneous powers p and q. The transient between capacitive and inductive operation is very fast, with a settling time for the reactive power of less than one third of the fundamental period. It is important to emphasize that after $t = 0.25$ s, thanks to the injection of the optimal third-harmonic circulating current, the LC-StatCom is able to provide sinusoidal currents despite operating at 100% rated power inductive mode. Unlike in [15] where transitions need to occur at zero current to allow for safe disconnection and connection of the compensating inductor, transitions can happen at any time instant with the proposed method.

Also, Fig. 10 shows that the active power p, which is associated with the converter efficiency, does not vary significantly before and after the operation change at $t = 0.25$ s. In this case,

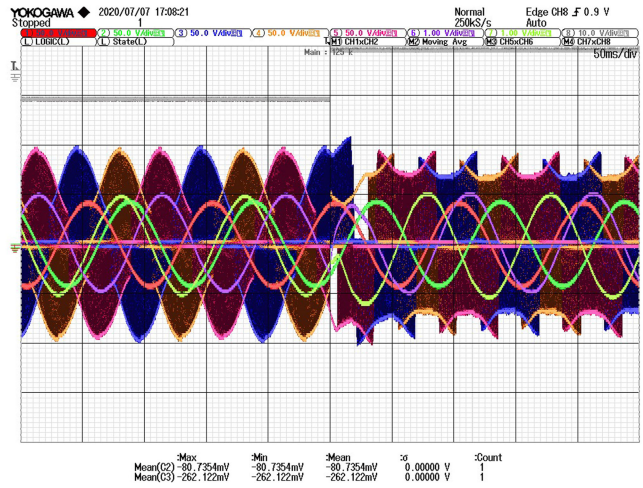

Fig. 11. Experimental waveforms of ac-side PWM converter voltages v_{ab}, v_{bc}, and v_{ca} (CH3, CH4, and CH5), line-to-neutral grid voltages e_a and e_b (CH1 and CH2), and injected StatCom currents i_a and i_b (CH7 and CH6), during a sudden reactive power change from 100% rated power capacitive mode to 100% rated power inductive mode in the middle of the oscilloscope screen, i.e., at $t = 0.25$ s.

the injection of the proposed optimal third-harmonic circulating current does not affect significantly the ratio between provided reactive power and consumed active power.

The oscilloscope result corresponding to Figs. 7–10 is shown in Fig. 11.

Consequently, experimental measurements validate the proposed method that allows the LC-StatCom to operate at full inductive range.

VI. Complimentary Simulations

In this section, additional simulation results for a 36-MVA multilevel LC-StatCom with five submodules per phase are provided to show the effectiveness of the proposed method to enhance inductive operation when multiple submodules are used. The parameters of the simulated system are the same (in per-unit system) to those used in the experiment (given in Table I), but for a 6-kV 50-Hz grid. A phase-shifted carrier PWM strategy [31] with 1-kHz carriers has been adopted. The system is simulated in MATLAB/Simulink environment.

The waveforms for the case when reactive power $q^\star$ changes from 100% rated power capacitive mode to 100% rated power inductive mode at $t = 0.02$ s are shown in Fig. 12.

Similar to the experimental results (shown in Figs. 7–10), the compensated LC-StatCom has capability to regulate the capacitor voltages and arm currents with smooth transients. Prior to $t = 0.02$ s, in 100% capacitive mode, the circulating current is almost zero due to the balanced system operation, whereas from $t = 0.02$ s, in 100% inductive mode, the optimal third-harmonic circulating current begins to be injected in order to suitably shape the capacitor voltages. It is important to note that the individual capacitor voltages are balanced, and their maximums are regulated to the upper bound V_{UB}. The proposed third-harmonic

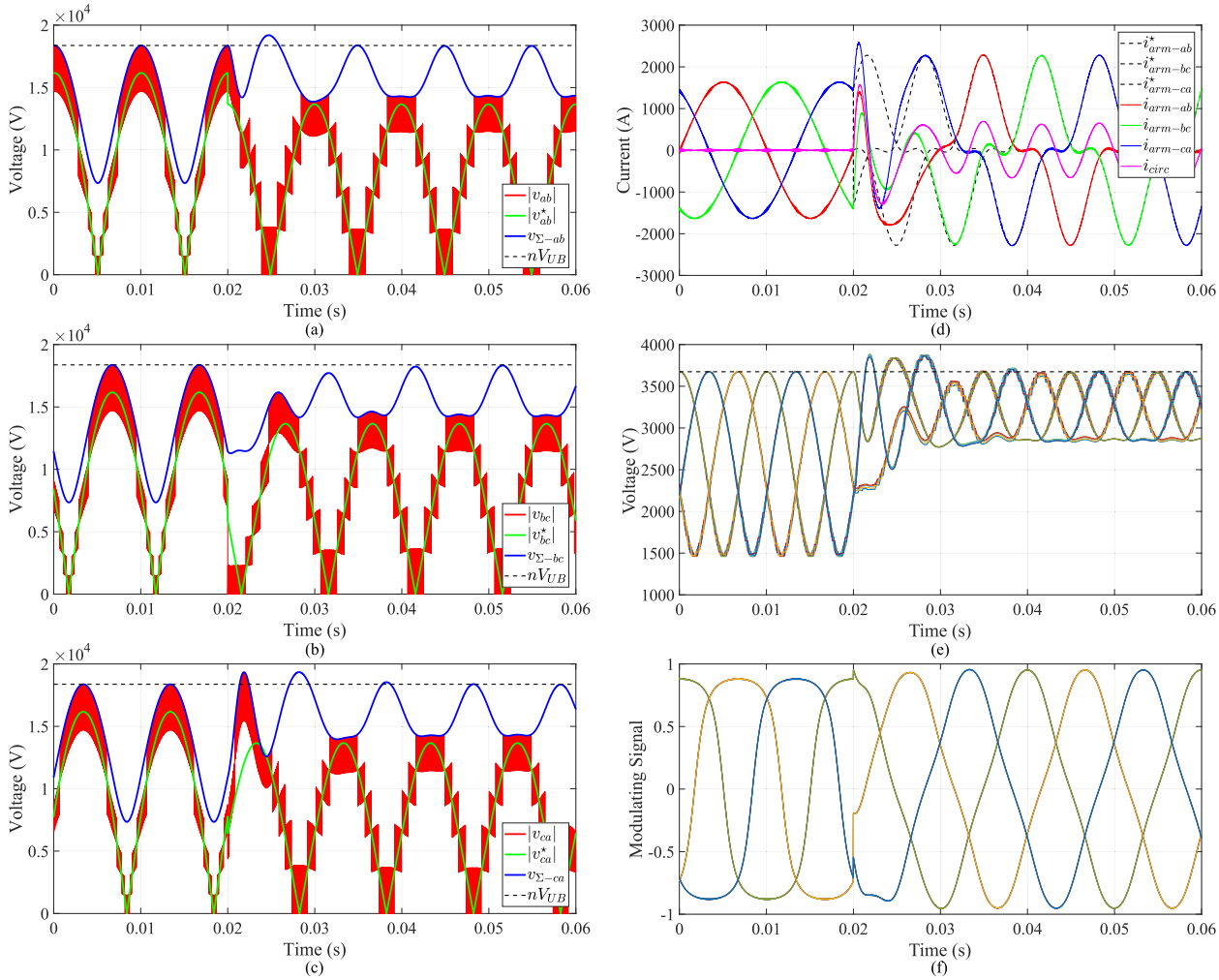

Fig. 12. LC-StatCom simulation waveforms during a sudden reactive power change from 100% rated power capacitive-mode to 100% rated power inductive mode at $t = 0.02$ s. (a) Phase arm ab voltages v_{ab} and $v_{\Sigma-ab}$. (b) Phase arm bc voltages v_{bc} and $v_{\Sigma-bc}$. (c) Phase arm ca voltages v_{ca} and $v_{\Sigma-ca}$. (d) Arm currents $i_{\text{arm}-ab}$, $i_{\text{arm}-bc}$, and $i_{\text{arm}-ca}$. (e) Fifteen individual capacitor voltages. (f) Fifteen individual modulating signals.

circulating current shapes the individual capacitor voltages such that the individual modulating signals are in the range $[-1,\ 1]$.

The simulation results are in agreement with the experimental results shown in Section V, thus corroborating that the proposed method can be applied when multiple submodules are used.

VII. Conclusion

An optimal third-harmonic circulating current injection method has been developed for three-phase LC-StatComs with delta configuration for the purpose of increasing the range of operation to full inductive mode. The derivation of optimal third-harmonic circulating current is based on a thorough analysis of LC-StatCom dynamic behavior in the steady state. The proposed method minimizes the required circulating current magnitude under constraints on modulating signal range and a prescribed upper bound on the capacitor voltages. Experimental results in a laboratory prototype validate the described approach and corroborate that the proposed optimal third-harmonic injected current method allows us to extend the range of operation of LC-StatComs to full inductive range. Reformulation of the proposed optimal circulating current injection concept to consider unbalanced converter operational conditions is a future direction for research to complement this article.

Appendix
Analytical Expressions for α_i and β_i Coefficients

This Appendix provides the α_i and β_i coefficients needed to calculate the amplitude A_i and phase ψ_i according to (29). With this information, one can calculate the shaped cluster voltage references in (28), ac-side converter voltage references in (30), and matrix A_c and vector b_c of the linear programming problem in (31).

References

[1] G. Farivar, B. Hredzak, and V. G. Agelidis, "Reduced-capacitance thin-film H-bridge multilevel STATCOM control utilizing an analytic filtering scheme," *IEEE Trans. Ind. Electron.*, vol. 62, no. 10, pp. 6457–6468, Oct. 2015.

[2] G. Farivar, C. D. Townsend, B. Hredzak, J. Pou, and V. G. Agelidis, "Low-capacitance cascaded h-bridge multilevel StatCom," *IEEE Trans. Power Electron.*, vol. 32, no. 3, pp. 1744–1754, Mar. 2017.

[3] T. Isobe, L. Zhang, R. Iijima, H. Tadano, Y. Kawanami, and K. Terazono, "Experimental verification of capacitance reduction in MMC-based STATCOM," in *Proc. Energy Convers. Congr. Expo.*, 2016, pp. 1–7.
[4] T. Isobe, D. Shiojima, K. Kato, Y. R. R. Hernandez, and R. Shimada, "Full-bridge reactive power compensator with minimized-equipped capacitor and its application to static VAR compensator," *IEEE Trans. Power Electron.*, vol. 31, no. 1, pp. 224–234, Jan. 2016.
[5] X. Ge and F. Gao, "Flexible third harmonic voltage control of low capacitance cascaded H-bridge STATCOM," *IEEE Trans. Power Electron.*, vol. 33, no. 3, pp. 1884–1889, Mar. 2018.
[6] D. Niu *et al.*, "Cascaded packed U-cell STATCOM with low capacitance and its third harmonic control," in *Proc. IEEE Appl. Power Electron. Conf. Expo.*, Jun. 2020, pp. 529–534.
[7] H. Wang and F. Blaabjerg, "Reliability of capacitors for DC-link applications in power electronic converters—An overview," *IEEE Trans. Ind. Appl.*, vol. 50, no. 5, pp. 3569–3578, Sep./Oct. 2014.
[8] R. Maheshwari, S. Munk-Nielsen, and S. Busquets-Monge, "Design of neutral-point voltage controller of a three-level NPC inverter with small DC-link capacitors," *IEEE Trans. Ind. Electron.*, vol. 60, no. 5, pp. 1861–1871, May 2013.
[9] B. Karanayil, V. G. Agelidis, and J. Pou, "Evaluation of dc-link decoupling using electrolytic or polypropylene film capacitors in three-phase grid-connected photovoltaic inverters," in *Proc. 39th Annu. Conf. IEEE Ind. Electron. Soc.*, Nov. 2013, pp. 6980–6986.
[10] T. Isobe, L. Zhang, H. Tadano, J. A. Suul, and M. Molinas, "Control of DC-capacitor peak voltage in reduced capacitance single-phase STATCOM," in *Proc. IEEE 17th Workshop Control Model. Power Electron.*, Jun. 2016, pp. 1–8.
[11] Z. He, L. Zhang, T. Isobe, and H. Tadano, "Dynamic performance improvement of single-phase STATCOM with drastically reduced capacitance," in *Proc. IEEE 3rd Int. Future Energy Electron. Conf. ECCE Asia*, Jun. 2017, pp. 1413–1418.
[12] G. Farivar, J. Pou, and A. Tripathi, "LC-StatCom with symmetrical I-V characteristic—Power loss analysis," in *Proc. 19th Eur. Conf. Power Electron. Appl.*, Sep. 2017, pp. 1–10.
[13] G. Farivar, J. Pou, and A. T., "LC-StatCom with symmetrical I-V characteristic: Total harmonic distortion study," in *Proc. Asian Conf. Energy, Power Transp. Electrific.*, Oct. 2017, pp. 1–5.
[14] G. Farivar *et al.*, "Load adaptive cascaded H-bridge low capacitance statcom with modular capacitors," in *Proc. 45th Ann. Conf. IEEE Ind. Electron. Soc.*, Lisbon, Portugal, 2019, pp. 3541–3546, doi: 10.1109/IECON.2019.8926951.
[15] G. Farivar, C. D. Townsend, B. Hredzak, J. Pou, and V. G. Agelidis, "Passive reactor compensated cascaded H-bridge multilevel LC-StatCom," *IEEE Trans. Power Electron.*, vol. 32, no. 11, pp. 8338–8348, Nov. 2017.
[16] G. Farivar, C. Townsend, J. Pou, and B. Hredzak, "Low-capacitance StatCom with modular inductive filter," *IEEE Trans. Power Electron.*, vol. 34, no. 4, pp. 3192–3203, Apr. 2019.
[17] Y. Jeon *et al.*, "An enhanced static compensator with DC-link voltage shaping method," IEEE Trans. Power Electron, vol. 35, no. 3, pp. 2488–2500, Mar. 2020.
[18] M. Hagiwara, R. Maeda, and H. Akagi, "Negative-sequence reactive-power control by a PWM STATCOM based on a modular multilevel cascade converter (MMCC-SDBC)," *IEEE Trans. Ind. Appl.*, vol. 48, no. 2, pp. 720–729, Mar./Apr. 2012.
[19] T. Tanaka, H. Wang, and F. Blaabjerg, "A DC-link capacitor voltage ripple reduction method for a modular multilevel cascade converter with single delta bridge cells," *IEEE Trans. Ind Appl.*, vol. 55, no. 6, pp. 6115–6126, Nov./Dec. 2019.
[20] Z. Li, R. Lizana, S. M. Lukic, A. V. Peterchev, and S. M. Goetz, "Current injection methods for ripple-current suppression in delta-configured split-battery energy storage," *IEEE Trans. Power Electron.*, vol. 34, no. 8, pp. 7411–7421, Aug. 2019.
[21] H. Zhixing *et al.*, "Circulating current derivation and comprehensive compensation of cascaded STATCOM under asymmetrical voltage conditions," *IET Gener., Transmiss. Distrib.*, vol. 10, no. 12, pp. 2924–2932, 2016.
[22] J. Pou, S. Ceballos, G. Konstantinou, V. G. Agelidis, R. Picas, and J. Zaragoza, "Circulating current injection methods based on instantaneous information for the modular multilevel converter," *IEEE Trans. Ind. Electron.*, vol. 62, no. 2, pp. 777–788, Feb. 2015.
[23] E. Behrouzian and M. Bongiorno, "Investigation of negative-sequence injection capability of cascaded H-bridge converters in star and delta configuration," *IEEE Trans. Power Electron.*, vol. 32, no. 2, pp. 1675–1683, Feb. 2017.
[24] E. R. Ramos, R. Leyva, G. G. Farivar, H. D. Tafti, C. D. Townsend, and J. Pou, "Incremental passivity control in multilevel cascaded H-bridge converters," *IEEE Trans. Power Electron.*, vol. 35, no. 8, pp. 8766–8778, Aug. 2020.
[25] R. Darus, J. Pou, G. Konstantinou, S. Ceballos, R. Picas, and V. G. Agelidis, "A modified voltage balancing algorithm for the modular multilevel converter: Evaluation for staircase and phase-disposition PWM," *IEEE Trans. Power Electron.*, vol. 30, no. 8, pp. 4119–4127, Aug. 2015.
[26] G. Konstantinou, H. R. Wickramasinghe, S. Ceballos, and J. Pou, "Submodule voltage balancing and loss equalisation in alternate arm converters based on virtual voltages," in *Proc. Int. Power Electron. Conf.*, May 2018, pp. 3117–3122.
[27] E. Rodriguez, G. G. Farivar, J. Pou, H. D. Tafti, C. D. Townsend, and S. Vazquez, "A generalized voltage balancing algorithm for modular multilevel cascaded converters," in *Proc. IEEE Energy Convers. Congr. Expo.*, Sep. 2019, pp. 214–218.
[28] M. Moosavi, G. Farivar, H. Iman-Eini, and S. M. Shekarabi, "A voltage balancing strategy with extended operating region for cascaded H-bridge converters," *IEEE Trans. Power Electron.*, vol. 29, no. 9, pp. 5044–5053, Sep. 2014.
[29] E. Rodriguez *et al.*, "Closed-loop analytic filtering scheme of capacitor voltage ripple in multilevel cascaded H-bridge converters," *IEEE Trans. Power Electron.*, vol. 35, no. 8, pp. 8819–8832, Aug. 2020.
[30] G. Farivar *et al.*, "Cascaded H-bridge low capacitance static compensator with modular switched capacitors," in *Proc. IEEE Trans. Ind. Electron.*, to be published, doi: 10.1109/TIE.2020.2992976.
[31] G. Farivar, B. Hredzak, and V. G. Agelidis, "Decoupled control system for cascaded H-bridge multilevel converter based STATCOM," *IEEE Trans. Ind. Electron.*, vol. 63, no. 1, pp. 322–331, Jan. 2016.

Ezequiel Rodriguez (Student Member, IEEE) was born in Tarragona, Spain, in 1994. He received the bachelor's degree in electrical engineering and the master's degree in engineering and technology of electronic systems (with first class hons. for both degrees, topping the 2012 and 2016 graduating cohort as valedictorian) from Universitat Rovira i Virgili, Tarragona, in 2016 and 2017, respectively. He is currently working toward the Ph.D. degree with the School of Electrical and Electronic Engineering, Nanyang Technological University, Singapore.

His research interests include modeling and control of power electronic converters, with an emphasis on modular multilevel cascade converters.

Ramon Leyva (Senior Member, IEEE) received the M.Sc. and Ph.D. degrees in telecommunication engineering from the Universitat Politecnica de Catalunya, Barcelona, Spain, in 1992 and 2000, respectively.

He was a Visiting Professor with LAAS-CNRS, Toulouse, France, in 2002–2003, 2009, and 2010, and with the COPEC–University of Colorado at Boulder, Boulder, CO, USA, in 2012. He is currently an Associate Professor with the Departament d'Enginyeria en Electronica, Electrica i Automatica, Universitat Rovira i Virgili, Tarragona, Spain. He has coauthored more than 100 scientific publications, two books. and one patent. He has been involved in more than 20 R&D projects. He serves as reviewer for several IEEE and IET scientific publications. His research interests include nonlinear and robust control of power converters and renewable energy.

Prof. Levya serves as reviewer for several IEEE and IET scientific publications.

Liu Qingxiang (Student Member, IEEE) received the B.Sc. degree in electrical engineering from Wuhan University, Wuhan, China, in 2018, and the M.Sc. degree in power electronics in 2019 from Nanyang Technological University, Singapore, where he is currently working toward the Ph.D. degree with the Interdisciplinary Graduate Program.

His research interests include modulation and control of power converters, multilevel converters, and flexible ac transmission system devices.

Christopher D. Townsend (Member, IEEE) received the B.E. and Ph.D. degrees in electrical engineering from the University of Newcastle, Callaghan NSW, Australia, in 2009 and 2013, respectively.

Subsequently, he spent three years working with ABB Corporate Research, Sweden, working on next-generation high-power converter technologies. Since then, he has held various postdoctoral research positions with the University of New South Wales, Sydney, NSW; the University of Newcastle; and Nanyang Technological University, Singapore. In 2019, he joined the Department of Electrical, Electronic and Computer Engineering, University of Western Australia, Crawley WA, Australia, as a Senior Lecturer. He has authored more than 60 published technical papers and has been involved in several industrial projects and educational programs in the field of power electronics. His research interests include topologies and modulation strategies for multilevel converters applied in power systems, renewable energy integration, and electric vehicle applications.

Dr. Townsend is a member of the IEEE Power Electronics Society and the IEEE Industrial Electronics Society.

Glen G. Farivar (Senior Member, IEEE) received the B.Sc. degree in electrical engineering from the Nooshirvani Institute of Technology, Babol, Iran, in 2008, the M.Sc. degree in power electronics from the University of Tehran, Tehran, Iran, in 2011, and the Ph.D. degree in electrical engineering from the University of New South Wales, Sydney, NSW, Australia, in 2016.

He is currently a Postdoctoral Research Fellow with the Energy Research Institute, Nanyang Technological Institute, Singapore. His research interests include renewable energy systems, high-power convertors, energy storage, flexible ac transmission system devices, and hybrid electric vehicles.

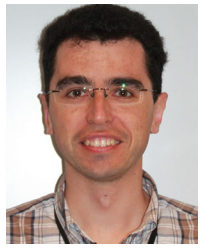

Salvador Ceballos received the M.S. degree in physics from the University of Cantabria, Santander, Spain, in 2001, and the M.S. and Ph.D. degrees in electronic engineering from the University of the Basque Country, Bilbao, Spain, in 2002 and 2008, respectively.

Since 2002, he has been with Tecnalia Research and Innovation, Derio, Spain, where he is currently a Principal Researcher with the Energy and Environment Division. His research interests include multilevel converters for high- and medium-voltage applications, fault-tolerant power electronic topologies, renewable energy systems, and power systems with high penetration of power converters.

Josep Pou (Fellow, IEEE) received the B.S., M.S., and Ph.D. degrees in electrical engineering from the Technical University of Catalonia (UPC), Barcelona, Spain, in 1989, 1996, and 2002, respectively.

In 1990, he joined the Faculty of UPC, as an Assistant Professor and became an Associate Professor in 1993. From February 2013 to August 2016, he was a Professor with the University of New South Wales (UNSW), Sydney, NSW, Australia. He is currently a Professor with the Nanyang Technological University (NTU), Singapore, where he is the Program Director of Power Electronics with the Energy Research Institute and the Co-Director of the Rolls-Royce with NTU Corporate Lab. From February 2001 to January 2002, and from February 2005 to January 2006, he was a Researcher with the Center for Power Electronics Systems, Virginia Tech, Blacksburg, VA, USA. From January 2012 to January 2013, he was a Visiting Professor with the Australian Energy Research Institute, UNSW, Sydney. He has authored more than 350 published technical papers and has been involved in several industrial projects and educational programs in the fields of power electronics and systems. His research interests include modulation and control of power converters, multilevel converters, renewable energy, energy storage, power quality, HVdc transmission systems, and more-electrical aircraft and vessels.

Dr. Pou was the recipient of the 2018 IEEE Bimal Bose Award for Industrial Electronics Applications in Energy Systems. He is an Associate Editor for the IEEE JOURNAL OF EMERGING AND SELECTED TOPICS IN POWER ELECTRONICS. He was a Co-Editor-in-Chief and an Associate Editor for the IEEE TRANSACTIONS ON INDUSTRIAL ELECTRONICS.